CrystEngComm

HIGHLIGHT

View Article Online
View Journal | View Issue

Cite this: *CrystEngComm*, 2025, **27**, 2795

Molecular beam epitaxy of AlGaN nanowires: source configuration and correlated material properties and device characteristics

Songrui Zhao

Semiconductor nanowires have emerged as an appealing material platform for cutting-edge semiconductor devices. Behind the exciting progress of semiconductor nanowire devices is the advancement in the understanding of the nanowire synthesis process and mechanism. In this article, I will focus on the recent development in the molecular beam epitaxy (MBE) of semiconductor aluninum gallium nitride (AlGaN) nanowires. MBE has become an attractive tool for large-scale semiconductor nanowire devices, whereas AlGaN is a technologically important semiconductor material for short-wavelength photonics, as well as high-power and radio-frequency (RF) electronics. Different from epilayers wherein only a horizontal surface is involved in the epitaxy, the epitaxial growth of nanowires in general involves both horizontal and vertical surfaces. Such a unique geometry, coupled with different source configurations, greatly affects the growth kinetics, and consequently the material properties and device characteristics. In this regard, the general considerations of MBE chamber configuration for epilayers are discussed first as the basics to understand the nanowire growth. This is followed by the uniqueness of nanowires. In the end, the experimental results regarding to the correlation of source configuration to AlGaN nanowire properties and device characterics such as alloy composition, optical properties, and light emission are discussed. This article could provide useful insight for the development of AlGaN nanowire devices as well as other epitaxial semiconductor nanowire devices beyond AlGaN, especially when the chamber configuration is considered. This article could also shed new light on explaining some features in semiconductor nanowires.

Received 11th February 2025,
Accepted 19th March 2025

DOI: 10.1039/d5ce00147a

rsc.li/crystengcomm

1. Introduction

The past decades have witnessed a lot of exciting developments of semiconductor nanowire devices. Some examples include lasers, photodetectors, transistors, and other emerging devices.[1–10] These advances in semiconductor nanowire devices are attributed to the improvement in understanding the synthesis of semiconductor nanowires, controlling the formation of nanowires in a highly precise manner, as well as the benefits of nanowires compared to their planar counterparts such as better strain relaxation.[11]

Among various approaches to synthesize nanowires, using large epitaxial tools has received more and more attention due to the potentially offered compatibility with the existing epitaxial semiconductor device fabrication processes. Epitaxially formed nanowires could be an important step toward the penetration of nanowire devices into practical semiconductor devices in electronics and photonics.

From the materials viewpoint, one important family is the III-nitrides, which have been used for various commercial electronic and photonic devices, *e.g.*, light bulbs based on InGaN light-emitting diodes (LEDs), fast chargers based on GaN power devices, and so on.[12–23] Adding Al to GaN further makes III-nitrides a unique semiconductor material platform for ultraviolet (UV) photonics, as well as high-power and RF

Department of Electrical and Computer Engineering, McGill University, 3480 University Street, Montreal, QC H3A0E9, Canada. E-mail: songrui.zhao@mcgill.ca

Songrui Zhao is an Associate Professor in the Department of Electrical and Computer Engineering and Associate Member in the Department of Physics at McGill University. His current research interests include molecular beam epitaxy of III-nitride nanostructures and their applications to light emitting, light detection, and photocatalysis for information processing, sensing, and renewable energy. He is the recipient of several awards, including the International Conference on MBE Young Investigator Award in 2018 (conferred every two years with one awardee), the North American MBE Young Investigator Award in 2022 (conferred every year with one awardee), and IDW24 Best Paper Award in 2024.

electronics.[13,18,19,24–29] These advantages of III-nitrides, together with the intrinsic merits of nanowires, make III-nitride nanowires a highly appealing material platform for device developments.

Indeed, the past decade has witnessed a significant growth in the study of epitaxial III-nitride nanowires and their device applications with both metal–organic chemical vapor deposition (MOCVD) and MBE, and numerous review articles have been written, highlighting the research progress, *e.g.*, ref. 30–38. Some of the key device developments include the shortest wavelength (207 nm) LEDs using AlN nanowires,[39] single photon sources,[40] surface emitting lasers in the UV and visible,[41–44] electrically pumped deep UV lasers down to 239 nm,[45,46] novel photodetectors,[47–50] as well as using III-nitride nanowires for artificial photosynthesis.[51–53]

In this minireview, I would like to focus on the MBE grown self-organized AlGaN nanowires. The general concept and characteristics of using MBE to grow epilayers and nanowires will also be discussed, as a necessary background and for the convenience of the readers. Moreover, the focus will be on the correlation between the chamber configuration and material properties as well as the device characteristics, which is often less reviewed in MBE books and literatures.[54–58]

On the other hand, it should be noted that while selective area epitaxy has become a more practical technique to control the nanowire size and distribution,[59–66] and *per se*, to achieve ultimate nanowire uniformity, the self-organized process remains the main drive for applications that do not require superior nanowire uniformity, *e.g.*, photocatalysts.[53] As such, being able to control the nanowire formation in the self-organized manner remains important.

2. General considerations of MBE chamber configuration for device-quality materials

In general, the MBE growth kinetics is highly dependent on the chamber configuration as well as the flux profile of the sources.[55,67–72] Dr. Wasilewski has studied these effects in detail in the epitaxy of III-V epilayers by correlating theoretical modelling and experiments based on a VG Semicon V90 MBE system.[67] The major findings are reviewed in this section, which will serve as the basics to understand the difference between the epitaxy of thin layers and nanowires.

Fig. 1(a) shows the flux modelling with a standard effusion cell loaded with a 30-cc conical shaped crucible in the V90 MBE system. The axial direction of the source has an angle of 45 degrees with respect to the substrate normal direction. It is seen that the flux profile is highly nonuniform on the virtual substrate. Consequently, if one would do an epitaxial growth without rotating the substrate, a thickness variation across the virtual substrate would be expected, as illustrated in Fig. 1(b). The source that is used for this simulated growth is also highlighted in a darker colour compared to other sources. For the thickness variation, a factor of two could be obtained on a 3″ wafer, which is also

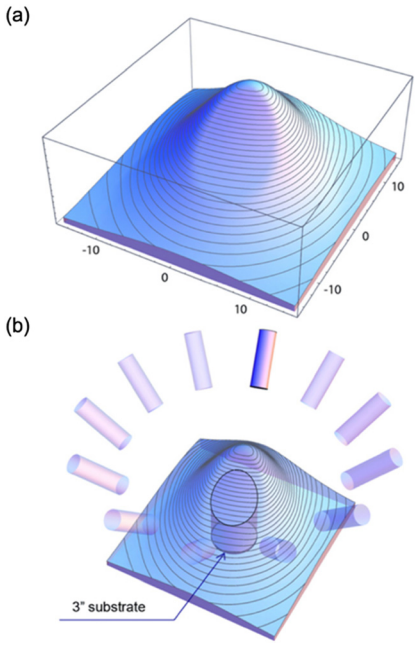

Fig. 1 (a) Simulated flux profile induced by a directional source, *i.e.*, the axial direction of the source has an angle with respect to the substrate normal direction, on a virtual substrate with a size of 30 cm × 30 cm. In this study, the angle is 45 degrees. (b) Simulated thickness profile of the epilayer grown on such a virtual substrate, considering the flux profile shown in (a). The virtual substrate is stationary.[67]

denoted in Fig. 1(b).[67] Rotating the substrate can reduce the thickness variation. Moreover, the substrate rotation speed (revolution per minute, rpm) needs to be carefully chosen, which is in particular the case of growing quantum cascade

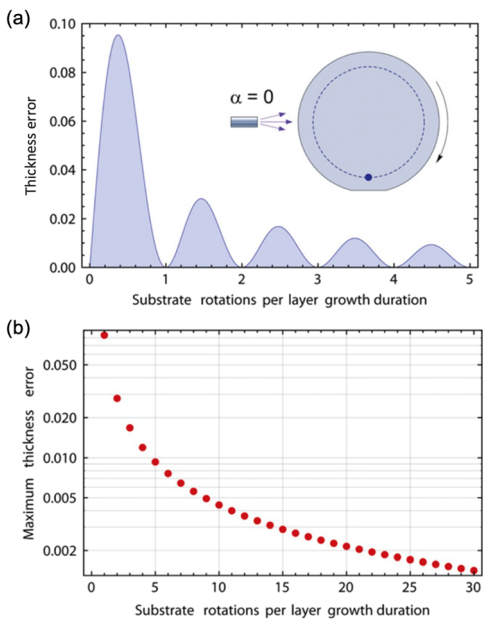

Fig. 2 (a) Simulated thickness error as a function of the substrate rotations per layer growth duration. (b) Maximum thickness error *versus* the substrate rotations per layer growth duration. Modification with permission from ref. 67.

laser (QCL) active layers, wherein typically around 100 pairs of nanometre-thick layers are needed.[67,73–76]

Fig. 2(a) illustrates the calculated thickness error compared to a given target thickness for a spot that is around 30 mm away from the wafer centre during GaAs growth on a 3″ wafer. It is seen that minimum errors can be achieved when the substrate rotates integer number of turns per layer growth duration, and half turns lead to large thickness errors.[67] It is also seen that for large substrate rotation numbers per layer growth duration, the thickness error reduces even for half turns – this can be seen more clearly in Fig. 2(b). This implies that high substrate rotation speed is always favourable, in order to achieve uniform layers. However, the stress on the substrate motor at high substrate rotation speed needs to be considered.

The source configuration can affect the choice of the substrate rotation speed considerably.[67] Fig. 3 illustrates the case of growing thin AlGaAs layers for QCLs, wherein Al and Ga sources are located at different relative positions (and their axes are around 45 degrees with respect to the substrate normal direction). It is seen that when Al and Ga are next to each other, the restriction on the substrate rotation speed is much relaxed for achieving a relatively uniform AlGaAs composition, whereas when Al and Ga sources are opposite to each other, the substrate rotation speed needs to be carefully chosen, otherwise a large compositional fluctuation will be introduced. As such, to achieve compositionally uniform thin layers, it is in general suggested to have the layer thickness equal to the integer number of monolayers (MLs) and in the meantime, have an integer number of turns during the ML deposition time.[67]

These findings highlight the critical role of the source configuration on the growth kinetics, as well as how to mitigate the nonuniformities (*e.g.*, thickness, composition) using a proper substrate rotation speed. On a separate note, the substrate rotation speed has also been found to affect the formation of ultrathin GaN quantum disks in nanowires.[77]

Lastly, it is noted that the angle between the axial direction of the source and the normal direction of the substrate needs to be optimized, in order to reduce the thickness variation maximally when rotating the substrate. This angle is typical in the range of 30 to 45 degrees, depending on the detailed system design and varying across different manufacturers.[71,78] It is further noted that, while the state of the art thickness variation is around 0.5% or less (from wafer centre to wafer edge) on a 3″ wafer, the typical thickness variation could be around 3%,[67] due to the complexity in the system design (and thus the flux uniformity is sometimes compromised).

3. Uniqueness of nanowires

Different from the epitaxy of thin layers wherein only a horizontal surface is involved, the epitaxy of nanowires generally involves an additional surface – the sidewall (a vertical surface). This unique geometry of nanowires, coupled with different source configurations, can drastically affect the growth kinetics and consequently the material properties and device characteristics.

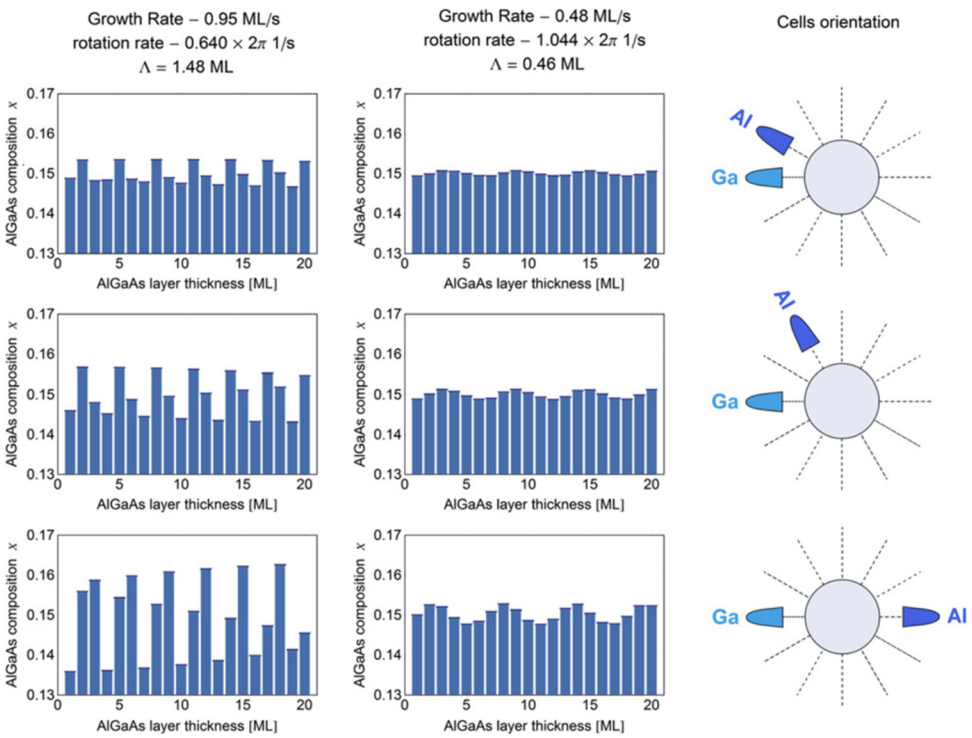

Fig. 3 Illustration of using a properly designed substrate rotation speed to minimize the effect of non-optimized source configuration for compositionally uniform AlGaAs thin layers.[67]

In this section, I will discuss the MBE growth of GaN nanowires as an example. The geometric model for the MBE growth of GaN nanowires is described first, followed by the effect of the source configuration on the GaN nanowire morphology.

3.1. The geometric model

Over the past decade, quite elegant understanding has been developed with respect to the MBE growth of GaN nanowires. It is generally agreed that the anisotropy of surface energies, together with a geometric model, largely drives the nanowire vertical growth.[68,70,71,79,80] Moreover, the anisotropy of surface energies, coupled with local III/N ratio variations (could be induced by nanowire geometry, nanowire density, source configurations, substrate rotation, or other factors), can mostly explain the formation of various crystalline planes/different nanowire facets and nanowire morphologies.[66,81,82]

Fig. 4 shows the schematic of the geometric model, wherein α and β denote the flux incident angles for Ga and N, respectively. A simple geometric argument indicates that the ratio of the vertical growth rate to the lateral growth rate is $\pi/\tan(\alpha)$ when the substrate is rotated during the growth.[71] Namely, with a given incident angle of the N flux, a smaller α leads to a higher vertical growth rate to lateral growth rate ratio. This can be explained phenomenologically by the spread-out of the Ga adatoms (due to the substrate rotation) on the larger-area sidewall compared to the top surface, which tends to cause a higher growth rate vertically than laterally. This also implies that whether the substrate rotates or not makes a big difference on the nanowire morphology. Note that the growth rate difference here does not require any Ga or N diffusion.

Furthermore, due to the unique nanowire sidewall (in contrast to the planar structure wherein there is no such sidewall), the Ga adatoms can diffusion along the sidewall, which may further modify the growth kinetics. For example, the diffusion may enhance the vertical growth and suppress the lateral growth. Moreover, for a given point on the sidewall, as the substrate rotates, Ga and N may not arrive at the same time, as such, the growth on the sidewall may mimic the metal-modulated epitaxy (MME),[71,83] being a possible reason that the nanowire sidewall is typically highly smooth.

3.2. Source configuration

Galopin *et al.* have compared the MBE growth of GaN nanowires using a head-on N source (*i.e.*, $\beta = 0$ in Fig. 4) and a directional N source (*i.e.*, $\beta \neq 0$ in Fig. 4).[70] It is found that for the case of using the head-on N source, highly vertically aligned nanowires are formed, and the nanowires are not inversely tapered. In contrast, when the directional N source is used, the nanowires are noticeably inversely tapered. This, first of all, indicates a difference on the lateral growth and can be explained by that, for the head-on N source, the N/Ga ratio is high on the top surface but low on the sidewall, leading to almost no lateral growth. In addition, the diffused Ga adatoms from the sidewall can also contribute to the vertical growth. In contrast, for the directional N source, the N/Ga ratio on the top surface is significantly reduced, whereas the N/Ga ratio on the sidewall is increased. This reduces the vertical growth and enhances the lateral growth. Moreover, the higher N/Ga ratio on the sidewall also reduces the Ga desorption/diffusion along the sidewall, further enhancing the lateral growth. Secondly, the fact that the nanowires are tapered when a directional N source is used indicates a nonuniform lateral growth rate along the nanowire (from the nanowire bottom to the nanowire top).

Treeck *et al.* have further studied the growth of a GaN shell using MBE on a GaN nanowire template.[68] Experimentally, they have observed an enhanced shell formation in the nanowire top region and bottom region when there is no substrate rotation, and with the substrate rotation, an improved shell uniformity is obtained, as shown in Fig. 5(a). They have further investigated theoretically what if one changes the in-plane angle (β) between Ga and N while keeping the incident angle of N flux (α) the same (Fig. 5(b)) under different III/N ratios and substrate rotation speeds. It is found that the proximity of N to Ga enhances the shell uniformity, and high substrate rotation speeds and III/N ratios mimic increasing the proximity of N to Ga. These observations (both experimentally and theoretically) can be explained by the surface diffused Ga adatoms along the

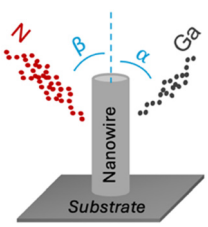

Fig. 4 Illustration of the geometric model for the MBE growth of GaN nanowires.

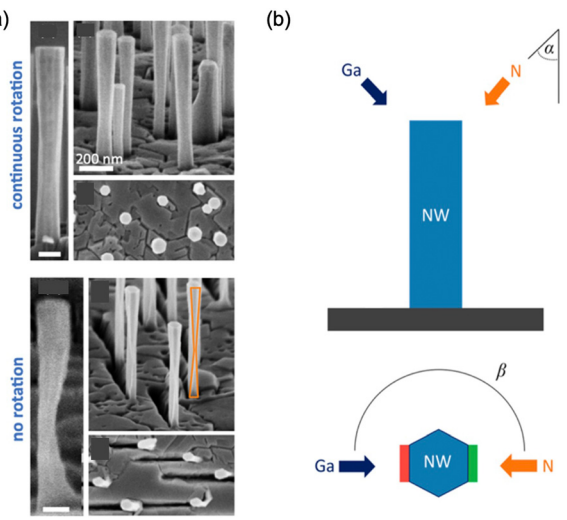

Fig. 5 (a) SEM images of GaN nanowires with a regrown GaN shell with and without substrate rotation. (b) The model used to explain the GaN shell formation. Modification with permission from ref. 68.

nanowire sidewall. Note that the enhanced shell formation in both the nanowire bottom and top regions could only be observed with low nanowire densities; for high nanowire densities, the shadow effect may suppress the formation of such shells.

4. AlGaN nanowires by MBE

Compared to binary compound semiconductors, the epitaxial kinetics of ternary compound semiconductors is more complicated. As an example, for AlGaN ternary compounds, the incorporation of Ga could be determined by the presence of Al, due to the much stronger Al–N bond compared to the Ga–N bond.[84] The difference in the bonding strength, together other factors such as surface features, will also affect the adatom diffusion kinetics along the nanowire sidewall during the MBE growth of AlGaN nanowires, leading to rich nanostructures such as AlGaN nanoclusters and Al-rich AlGaN shells. These features have been reviewed and discussed in depth previously, *e.g.*, ref. 85–88. In this section, I will discussion the recent studies on how this difference, coupled with different chamber configurations, affects the properties of AlGaN nanowires.

4.1. Effect of different Al sources

4.1.1. Ga incorporation kinetics. For this purpose, two Al sources at different locations are used.[89] The system configuration is shown in Fig. 6, wherein Al-I is close to the N source, and Al-II is further away from the N source. The axial direction of all sources has an angle of around 40 degrees with respect to the substrate normal direction. In the growth process, as Al-I is close to the N source, the impinged Al adatoms from Al-I can be captured quickly by the N source, leaving a minimum diffusion of Al adatoms along the nanowire sidewall at the growth front. In contrast, for Al-II, as it is further away from the N source, the Al adatoms from Al-II can diffuse more along the nanowire sidewall at the growth front. That said, when Al-I is used, Al adatoms tend to be incorporated more easily on the nanowire sidewall, favourable for the lateral growth; whereas when Al-II is used, Al adatoms tend to diffuse more easily along the nanowire sidewall, unfavourable for the lateral growth. This is also illustrated in Fig. 6.

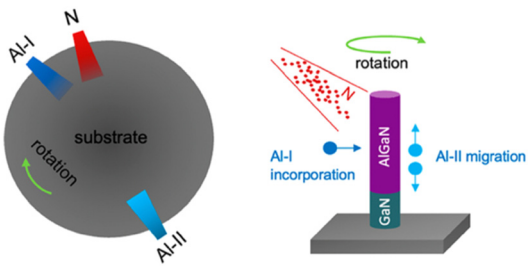

Fig. 6 Illustration of different Al adatom kinetics at the growth front when Al sources in two different locations are used.[89]

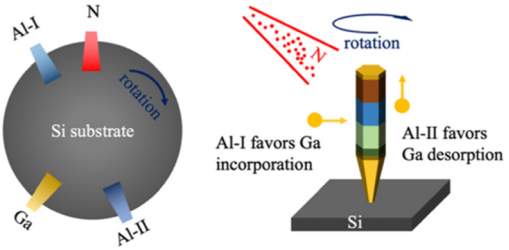

Fig. 7 Illustration of different Ga adatom kinetics at the growth front in the epitaxy of AlGaN nanowires, induced by Al sources in two different locations. Different colours within the nanowire denote different device layers.[85] The details are described in the main text when devices are discussed in section 4.1.4. The focus here is to illustrate Ga incorporation kinetics.

The difference in the lateral growth at the growth front may cause a drastic difference in the Ga incorporation and thus the properties of AlGaN nanowires. Note that at typical growth temperatures for AlGaN nanowires, Ga is highly desorbing. However, in the case when Al-I is used, the enhanced lateral growth will reduce the gaps amongst the nanowires at the growth front, which may in consequence suppress the Ga desorption from the nanowire sidewall and thus favour Ga incorporation; this is illustrated in Fig. 7. In contrast, when Al-II is used, the undermined lateral growth will increase the gaps amongst nanowires, which may in turn favour the Ga desorption from the nanowire sidewall at the growth front.

The difference in the lateral growth at the growth front may also cause different nanowire uniformities. Higher lateral growth rates may lead to more uniform nanowires, due to the possibly undermined diffusion of highly mobile adatoms on the nanowire sidewall. Lastly, it is important to note that the

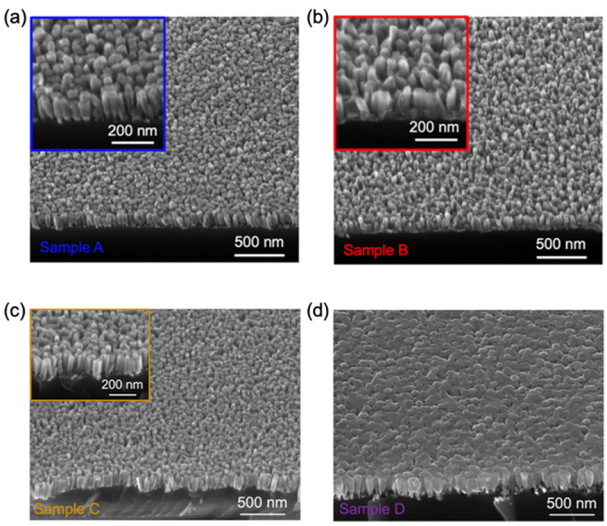

Fig. 8 SEM images of different AlGaN nanowire samples using different Al sources.[89] The insets are SEM images at higher magnifications. (a) Sample A is with Al-I. (b) Sample B is with Al-II. The difference between sample A and sample B is whether Al-I or Al-II is used. (c) Sample C is with Al-II but with optimized growth conditions. The details are explained in the main text. (d) Sample D is with Al-I. The difference between sample C and sample D is whether Al-I or Al-II is used.

discussions here are on bulk AlGaN nanowires rather than AlGaN quantum wells or quantum disks in nanowires.

4.1.2. Nanowire morphology. Fig. 8(a) and (b) are the scanning electron microscope (SEM) images of AlGaN nanowires grown using similar growth parameters, except that different Al sources are used, with sample A using Al-I and sample B using Al-II. It is seen that the AlGaN nanowires in sample A are more uniform compared to AlGaN nanowires in sample B, with respect to the nanowire height and diameter. The detailed nanowire statistics can be found in ref. 89. Furthermore, it would further be expected that if the nanowire morphology was optimized based on Al-II, using similar growth parameters but switching to Al-I could lead to a nanowire coalescence, due to the enhanced lateral growth at the growth front. It is indeed the case as revealed by the SEM images of sample C and sample D, shown in Fig. 8(c) and (d), respectively. Sample C is with Al-II, and growth parameters for sample C have been optimized to obtain similar morphology as that of sample A. Sample D is with Al-I but otherwise is similar to sample C in terms of growth parameters. Note that sample A and sample C have different growth conditions.

4.1.3. Alloy composition and optical properties. Room temperature photoluminescence (PL) experiments further indicate different Ga contents in AlGaN nanowires when the two different Al sources are used. Fig. 9(a) shows the room temperature (RT) PL of the four samples correlating to Fig. 8. First of all, nearly no PL is observed from sample D, due to the coalescence induced defects that are typically nonradiative recombination centres. Second, all other three samples show a PL peak around 210 nm, which is attributed to the presence of AlN nanoclusters.[39,85,90,91] Third, for sample A, a PL peak around 242 nm is observed, which is attributed to the PL emission from AlGaN. However, for sample B, which is grown using similar parameters as of sample A but using Al-II, only a very weak PL peak around 236 nm is observed, suggesting a low Ga content due to high Ga desorption. Sample C is the optimized (with respect to the nanowire morphology) AlGaN nanowire sample using Al-II and an AlGaN PL peak around 240 nm can be seen. The PL intensity difference compared to sample A could be related to the difference in the light extraction efficiency (either due to a slight change of the nanowire density or the variation of Al content). The estimated Al mole fractions for samples A, B, and C using the Vegard's law are 68%, 74%, and 71%, respectively.[92]

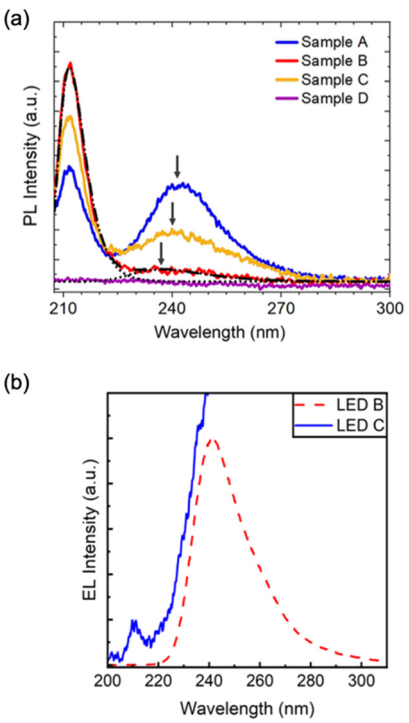

Fig. 9 (a) RTPL of different bulk AlGaN nanowire samples (*i.e.*, without any quantum wells or quantum disks) using different Al sources. Samples A, B, C, and D are the same samples as shown in Fig. 8 for SEM studies. The black dot/dash curves are deconvoluted PL peaks. The details on the PL experiments can be found in ref. 89. (b) RT EL of AlGaN nanowire LEDs, correlating to the schematic shown in Fig. 7, using the two different Al sources. The measurement details can be found in ref. 85. The LED identification (*i.e.*, LED B, LED C) from the original study is used. There are no correlations between LED B and sample B and between LED C and sample C.

4.1.4. Difference in LED device characteristics. AlGaN UV LED devices using the two different Al sources also exhibit drastically different electroluminescence (EL) characteristics. The device structure is schematically shown in Fig. 7, from bottom to top, it consists of n-GaN seeding layer (around 250 nm), GaN-based TJ, and AlGaN p–i–n homojunctions with thicknesses of 120 nm, 80 nm, and 120 nm for n-AlGaN, i-AlGaN, and p-AlGaN layers, respectively. A thin p-GaN contact layer (5–10 nm) finishes the complete device structure. The metallization process can be found in ref. 85. As shown in Fig. 9(b), LED B is the AlGaN nanowire UV LED device using Al-I and the designed EL emission around 240 nm is observed. On the other hand, if using similar growth parameters but switching to Al-II (LED C), the AlGaN EL peak is absent, whereas EL from pure AlN is observed. More detailed discussions on the EL emission characteristics of LED C, including the peak at 210 nm, can be found in ref. 85.

4.1.5. Further discussions. It is thus seen that, for self-organized AlGaN nanowires, if enhancing the Ga incorporation is the priority, it might be preferred that Al is placed next to N. This could be applied to the incorporation of highly desorbing dopant species in typical growth conditions as well, such as Mg. And then, to minimize compositional nonuniformity, Ga might be placed next to Al (see discussions in section 2). With this chamber configuration, it is noted though, the Al diffusion is compromised, which might not be favourable to achieve smooth AlN epilayers in metal-rich condition. However, other techniques such as MME could be used to mitigate this issue.[83]

On the other hand, recent years have witnessed a growing interest of using nanowires as dislocation density filters to obtain compact epilayers and devices, *e.g.*, ref. 93–98. The analysis here could provide insight on the chamber layout to enhance the nanowire coalescence.

In addition, the analysis here could also shed new light on explaining some features related to nanowires, such as

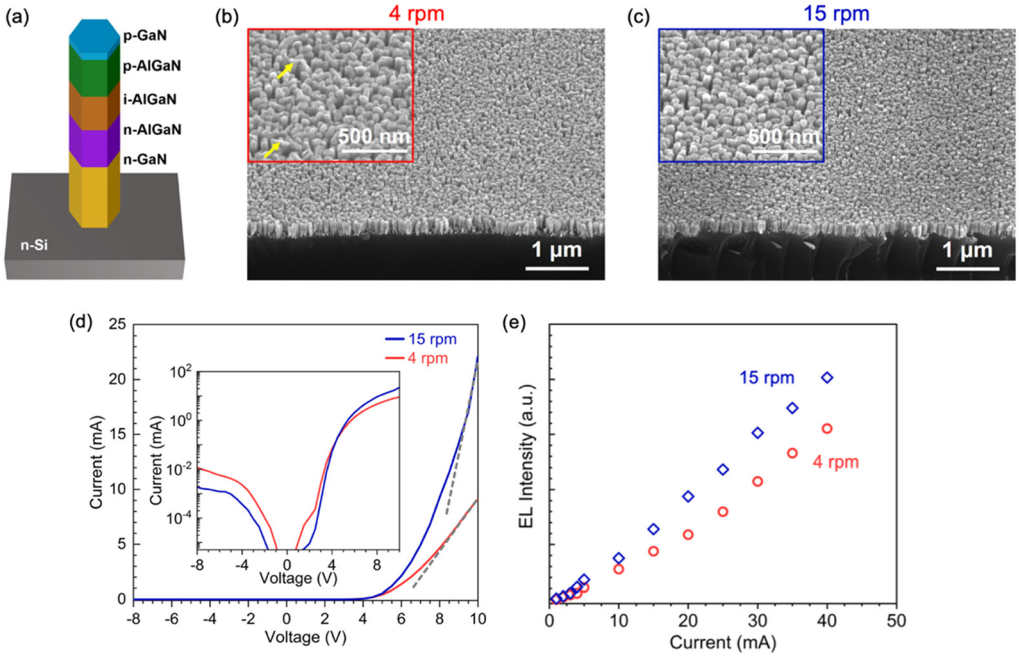

Fig. 10 (a) Schematic of the AlGaN nanowire UV LED structure used to investigate the substrate rotation speed. The insets are SEM images at higher magnifications. (b) and (c) SEM images of AlGaN nanowire LED structures grown at 4 rpm and 15 rpm, respectively. (d) and (e) The comparison of device characteristics. Details are described in the main text.[102]

compositional fluctuations in AlGaN nanowires,[86,87] compositional nonuniformities in InGaN nanowires,[99–101] and so on.

4.2. Substrate rotation

Fig. 10(a) shows the AlGaN p–i–n homojunction nanowire UV LED structure used to investigate the effect of the substrate rotation speed on the device characteristics. The thicknesses for n-GaN, n-AlGaN, i-AlGaN, p-AlGaN, p-GaN layers are around 100 nm, 40 nm, 40 nm, 40 nm, and 3 nm, respectively. Fig. 10(b) and (c) show the SEM images of the LED structures grown at 4 rpm and 15 rpm, respectively. It is seen that for the structure grown at 15 rpm, the nanowire uniformity is noticeably better, which can be explained by the geometric model described earlier. The detailed nanowire statistics can be found in ref. 102.

Fig. 10(d) shows the comparison of the I–V characteristics between the two types of AlGaN nanowire UV LEDs. It is seen that using 15 rpm can noticeably improve the forward current of the device. In the meantime, using 15 rpm can also improve the light output power, thanks to the improved nanowire uniformity at the higher substrate rotation speed.[102]

It has been shown earlier that for the epilayer growth of III–V materials, to minimize the adverse effect of the directional sources, as well as to "bypass" the effect of different source configurations, high and carefully chosen substrate rotation speed is necessary. It is further shown earlier that high rotation speed leads to a uniform GaN shell. Discussions in this section also indicate that high rotation speed improves the AlGaN nanowire uniformity and consequently the device performance. Therefore, it might be seen that, using high substrate rotation speed might always be favourable to mitigate non-ideal chamber configurations.

5. Concluding remarks

In summary, the recent advancement on the MBE grown AlGaN nanowires, which are an emerging material platform for UV photonics, as well as high-power and RF electronics, is discussed in this minireview. Compared to epilayers wherein only a horizontal surface is involved, the growth of nanowires is more complicated, due to the presence of an additional surface, *i.e.*, the sidewall of nanowires. This is further complicated by different source configurations, as well as different bonding strengths in ternary compound semiconductors. As such, the focus of this minireview is on the chamber configuration dependent material properties and device characteristics. Given the complexity of the ultrahigh vacuum (UHV) systems, it might be nearly impossible for one to vent the UHV growth chamber only for the source configuration dependent material properties and device characteristics investigation purpose. I hope this minireview can provide some useful insight for the material and device development using AlGaN nanowires and other semiconductor nanowires beyond AlGaN.

Data availability

Data is available upon reasonable request to the author.

Author contributions

This article is written by S. Z. without using any artificial intelligence (AI) tools.

Conflicts of interest

There are no conflicts to declare.

Acknowledgements

This work is supported by Natural Sciences and Engineering Research Council of Canada, Fonds de recherche du Québec – Nature et technologies, and McGill University.

Notes and references

1 Y. Liang, C. Li, Y. Z. Huang and Q. Zhang, *ACS Nano*, 2020, **14**, 14375–14390.
2 J. Meng and Z. Li, *Adv. Mater.*, 2020, **32**, e2000130.
3 T. A. Pham, A. Qamar, T. Dinh, M. K. Masud, M. Rais-Zadeh, D. G. Senesky, Y. Yamauchi, N. T. Nguyen and H. P. Phan, *Adv. Sci.*, 2020, **7**, 2001294.
4 X. Chen, B. Chen, B. Jiang, T. Gao, G. Shang, S. T. Han, C. C. Kuo, V. A. L. Roy and Y. Zhou, *Adv. Funct. Mater.*, 2022, **33**, 2208807.
5 Z. Li, Z. He, C. Xi, F. Zhang, L. Huang, Y. Yu, H. H. Tan, C. Jagadish and L. Fu, *Adv. Mater. Technol.*, 2023, **8**, 2202126.
6 S. Steinhauer, S. Gyger and V. Zwiller, *Appl. Phys. Lett.*, 2021, **118**, 100501.
7 K. Ren, C. Li, Z. Fang and F. Feng, *Laser Photonics Rev.*, 2023, **17**, 2200758.
8 W. Cao, H. Bu, M. Vinet, M. Cao, S. Takagi, S. Hwang, T. Ghani and K. Banerjee, *Nature*, 2023, **620**, 501–515.
9 K. Peng, D. Jevtics, F. Zhang, S. Sterzl, D. A. Damry, M. U. Rothmann, B. Guilhabert, M. J. Strain, H. H. Tan, L. M. Herz, L. Fu, M. D. Dawson, A. Hurtado, C. Jagadish and M. B. Johnston, *Science*, 2020, **368**, 510.
10 S. Zhao, in *Semiconductors and Semimetals*, ed. Z. Mi and H. H. Tan, ScienceDirect, 2024, vol. 116, p. 1.
11 F. Glas, *Phys. Rev. B: Condens. Matter Mater. Phys.*, 2006, **74**, r121302.
12 J. Y. Tsao, M. H. Crawford, M. E. Coltrin, A. J. Fischer, D. D. Koleske, G. S. Subramania, G. T. Wang, J. J. Wierer and R. F. Karlicek, *Adv. Opt. Mater.*, 2014, **2**, 809–836.
13 J. Y. Tsao, S. Chowdhury, M. A. Hollis, D. Jena, N. M. Johnson, K. A. Jones, R. J. Kaplar, S. Rajan, C. G. Van de Walle, E. Bellotti, C. L. Chua, R. Collazo, M. E. Coltrin, J. A. Cooper, K. R. Evans, S. Graham, T. A. Grotjohn, E. R. Heller, M. Higashiwaki, M. S. Islam, P. W. Juodawlkis, M. A. Khan, A. D. Koehler, J. H. Leach, U. K. Mishra, R. J. Nemanich, R. C. N. Pilawa-Podgurski, J. B. Shealy, Z. Sitar, M. J. Tadjer, A. F. Witulski, M. Wraback and J. A. Simmons, *Adv. Electron. Mater.*, 2018, **4**, 1600501.
14 D. Iida and K. Ohkawa, *Semicond. Sci. Technol.*, 2022, **37**, 013001.
15 M. S. Wong, J. S. Speck, S. Nakamura and S. P. DenBaars, *IEEE J. Quantum Electron.*, 2022, **58**, 1–11.
16 W. Y. Fu and H. W. Choi, *J. Appl. Phys.*, 2022, **132**, 060903.
17 J. Y. Lin and H. X. Jiang, *Appl. Phys. Lett.*, 2020, **116**, 100502.
18 H. Amano, R. Collazo, C. D. Santi, S. Einfeldt, M. Funato, J. Glaab, S. Hagedorn, A. Hirano, H. Hirayama, R. Ishii, Y. Kashima, Y. Kawakami, R. Kirste, M. Kneissl, R. Martin, F. Mehnke, M. Meneghini, A. Ougazzaden, P. J. Parbrook, S. Rajan, P. Reddy, F. Römer, J. Ruschel, B. Sarkar, F. Scholz, L. J. Schowalter, P. Shields, Z. Sitar, L. Sulmoni, T. Wang, T. Wernicke, M. Weyers, B. Witzigmann, Y.-R. Wu, T. Wunderer and Y. Zhang, *J. Phys. D: Appl. Phys.*, 2020, **53**, 503001.
19 H. Amano, Y. Baines, E. Beam, M. Borga, T. Bouchet, P. R. Chalker, M. Charles, K. J. Chen, N. Chowdhury, R. Chu, C. De Santi, M. M. De Souza, S. Decoutere, L. Di Cioccio, B. Eckardt, T. Egawa, P. Fay, J. J. Freedsman, L. Guido, O. Häberlen, G. Haynes, T. Heckel, D. Hemakumara, P. Houston, J. Hu, M. Hua, Q. Huang, A. Huang, S. Jiang, H. Kawai, D. Kinzer, M. Kuball, A. Kumar, K. B. Lee, X. Li, D. Marcon, M. März, R. McCarthy, G. Meneghesso, M. Meneghini, E. Morvan, A. Nakajima, E. M. S. Narayanan, S. Oliver, T. Palacios, D. Piedra, M. Plissonnier, R. Reddy, M. Sun, I. Thayne, A. Torres, N. Trivellin, V. Unni, M. J. Uren, M. Van Hove, D. J. Wallis, J. Wang, J. Xie, S. Yagi, S. Yang, C. Youtsey, R. Yu, E. Zanoni, S. Zeltner and Y. Zhang, *J. Phys. D: Appl. Phys.*, 2018, **51**, 163001.
20 C.-C. Lin, Y.-R. Wu, H.-C. Kuo, M. S. Wong, S. P. DenBaars, S. Nakamura, A. Pandey, Z. Mi, P. Tian, K. Ohkawa, D. Iida, T. Wang, Y. Cai, J. Bai, Z. Yang, Y. Qian, S.-T. Wu, J. Han, C. Chen, Z. Liu, B.-R. Hyun, J.-H. Kim, B. Jang, H.-D. Kim, H.-J. Lee, Y.-T. Liu, Y.-H. Lai, Y.-L. Li, W. Meng, H. Shen, B. Liu, X. Wang, K.-L. Liang, C.-J. Luo and Y.-H. Fang, *JPhys Photonics*, 2023, **5**, 042502.
21 A. Pandey, M. Reddeppa and Z. Mi, *Light: Adv. Manuf.*, 2023, **4**, 31.
22 Z. Li, Y. Liu, F. Feng, Z. Liu, M. Wong, H. S. Kwok and Z. Liu, *IEEE Open J. Immersive Disp.*, 2024, **1**, 62.
23 K. Behrman and I. Kymissis, *Nat. Electron.*, 2022, **5**, 564–573.
24 T. Takano, T. Mino, J. Sakai, N. Noguchi, K. Tsubaki and H. Hirayama, *Appl. Phys. Express*, 2017, **10**, 031002.
25 Z. Zhang, M. Kushimoto, T. Sakai, N. Sugiyama, L. J. Schowalter, C. Sasaoka and H. Amano, *Appl. Phys. Express*, 2019, **12**, 124003.
26 M. Kneissl, T.-Y. Seong, J. Han and H. Amano, *Nat. Photonics*, 2019, **13**, 233–244.
27 D. Li, K. Jiang, X. Sun and C. Guo, *Adv. Opt. Photonics*, 2018, **10**, 43.
28 T. D. Moustakas and R. Paiella, *Rep. Prog. Phys.*, 2017, **80**, 106501.
29 Q. Zhang, X. Yin and S. Zhao, *Phys. Status Solidi RRL*, 2021, **15**, 2100090.
30 S. Zhao and Z. Mi, *Crystals*, 2017, **7**, 268.

31 S. Zhao, H. P. T. Nguyen, M. G. Kibria and Z. Mi, *Prog. Quantum Electron.*, 2015, **44**, 14–68.
32 S. Zhao and Z. Mi, *IEEE J. Quantum Electron.*, 2018, **54**, 1–9.
33 M. Spies and E. Monroy, *Semicond. Sci. Technol.*, 2019, **34**, 053002.
34 F. Chen, X. Ji and S. P. Lau, *Mater. Sci. Eng., R*, 2020, **142**, 100578.
35 V. Vignesh, Y. Wu, S.-U. Kim, J.-K. Oh, C. Bagavath, D.-Y. Um, Z. Mi and Y.-H. Ra, *J. Inf. Disp.*, 2023, **25**, 13–59.
36 S. Zhao, J. Lu, X. Hai and X. Yin, *Micromachines*, 2020, **11**, 125.
37 J. Bosch, C. Durand, B. Alloing and M. Tchernycheva, *J. Inf. Disp.*, 2024, **25**, 61–73.
38 Y. Wu, X. Liu, A. Pandey, P. Zhou, W. J. Dong, P. Wang, J. Min, P. Deotare, M. Kira, E. Kioupakis and Z. Mi, *Prog. Quantum Electron.*, 2022, **85**, 100401.
39 S. Zhao, A. T. Connie, M. H. Dastjerdi, X. H. Kong, Q. Wang, M. Djavid, S. Sadaf, X. D. Liu, I. Shih, H. Guo and Z. Mi, *Sci. Rep.*, 2015, **5**, 8332.
40 M. J. Holmes, K. Choi, S. Kako, M. Arita and Y. Arakawa, *Nano Lett.*, 2014, **14**, 982–986.
41 Y.-H. Ra and C.-R. Lee, *Nano Energy*, 2021, **84**, 105870.
42 Y.-H. Ra, R. T. Rashid, X. Liu, S. M. Sadaf, K. Mashooq and Z. Mi, *Sci. Adv.*, 2020, **6**, eaav7523.
43 M. F. Vafadar and S. Zhao, *Sci. Rep.*, 2023, **13**, 6633.
44 M. F. Vafadar and S. Zhao, *ACS Nano*, 2024, **18**, 14290–14297.
45 S. Zhao, X. Liu, Y. Wu and Z. Mi, *Appl. Phys. Lett.*, 2016, **109**, 191106.
46 S. Zhao, X. Liu, S. Y. Woo, J. Kang, G. A. Botton and Z. Mi, *Appl. Phys. Lett.*, 2015, **107**, 043101.
47 M. Fathabadi and S. Zhao, *ACS Photonics*, 2023, **10**, 2825–2831.
48 M. Fathabadi and S. Zhao, *ACS Photonics*, 2023, **10**, 1969–1975.
49 M. Fathabadi, Y. Yin, S. Li and S. Zhao, *Adv. Opt. Mater.*, 2023, **12**, 2302372.
50 Y. Luo, D. Wang, Y. Kang, X. Liu, S. Fang, M. H. Memon, H. Yu, H. Zhang, D. Luo, X. Sun, B. S. Ooi, C. Gong, Z. Xu and H. Sun, *Adv. Opt. Mater.*, 2022, **10**, 2102839.
51 M. G. Kibria, F. A. Chowdhury, S. Zhao, B. AlOtaibi, M. L. Trudeau, H. Guo and Z. Mi, *Nat. Commun.*, 2015, **6**, 6797.
52 M. G. Kibria, S. Zhao, F. A. Chowdhury, Q. Wang, H. P. T. Nguyen, M. L. Trudeau, H. Guo and Z. Mi, *Nat. Commun.*, 2014, **5**, 3825.
53 P. Zhou, I. A. Navid, Y. Ma, Y. Xiao, P. Wang, Z. Ye, B. Zhou, K. Sun and Z. Mi, *Nature*, 2023, **613**, 66–70.
54 M. Henini, *Molecular Beam Epitaxy - From Research to Mass Production*, Elsevier, 1st edn, 2012.
55 J. Orton and T. Foxon, *Molecular beam epitaxy - a short history*, Oxford University Press, 2015.
56 M. Henini, *Molecular Beam Epitaxy - From Research to Mass Production*, Elsevier, 2nd edn, 2018.
57 M. A. Herman, W. Richter and H. Sitter, *Epitaxy: physical principles and technical implementation*, Springer Science & Business Media, 2013.
58 L. L. Chang and K. Ploog, *Molecular beam epitaxy and heterostructures*, Springer Science & Business Media, 2012.
59 K. A. Bertness, A. W. Sanders, D. M. Rourke, T. E. Harvey, A. Roshko, J. B. Schlager and N. A. Sanford, *Adv. Funct. Mater.*, 2010, **20**, 2911–2915.
60 A. Bengoechea-Encabo, F. Barbagini, S. Fernandez-Garrido, J. Grandal, J. Ristic, M. A. Sanchez-Garcia, E. Calleja, U. Jahn, E. Luna and A. Trampert, *J. Cryst. Growth*, 2011, **325**, 89–92.
61 K. Kishino, H. Sekiguchi and A. Kikuchi, *J. Cryst. Growth*, 2009, **311**, 2063–2068.
62 K. Yamano, K. Kishino, H. Sekiguchi, T. Oto, A. Wakahara and Y. Kawakami, *J. Cryst. Growth*, 2015, **425**, 316–321.
63 R. Wang, Y. H. Ra, Y. Wu, S. Zhao, H. P. T. Nguyen, I. Shih and Z. Mi, *Proc. SPIE*, 2016, **9748**, 9748IS.
64 Y.-H. Ra, R. T. Rashid, X. Liu, J. Lee and Z. Mi, *Adv. Funct. Mater.*, 2017, **27**, 1702364.
65 M. F. Vafadar and S. Zhao, *ACS Appl. Nano Mater.*, 2022, **5**, 16045–16050.
66 F. Pantle, M. Karlinger, S. Wörle, F. Becker, T. Höldrich, E. Sirotti, M. Kraut and M. Stutzmann, *J. Appl. Phys.*, 2022, **132**, 184304.
67 Z. R. Wasilewski, in *Molecular Beam Epitaxy - From Research to Mass Production*, ed. M. Henini, Elsevier, 1st edn, 2012, ch. 28.
68 D. van Treeck, S. Fernández-Garrido and L. Geelhaar, *Phys. Rev. Mater.*, 2020, **4**, 013404.
69 N. V. Sibirev, M. Tchernycheva, M. A. Timofeeva, J.-C. Harmand, G. E. Cirlin and V. G. Dubrovskii, *J. Appl. Phys.*, 2012, **111**, 104317.
70 E. Galopin, L. Largeau, G. Patriarche, L. Travers, F. Glas and J. C. Harmand, *Nanotechnology*, 2011, **22**, 245606.
71 C. T. Foxon, S. V. Novikov, J. L. Hall, R. P. Campion, D. Cherns, I. Griffiths and S. Khongphetsak, *J. Cryst. Growth*, 2009, **311**, 3423–3427.
72 F. Glas, *Phys. Status Solidi B*, 2010, **247**, 254–258.
73 A. Khalatpour, A. K. Paulsen, C. Deimert, Z. R. Wasilewski and Q. Hu, *Nat. Photonics*, 2020, **15**, 16–20.
74 S. Fujikawa, T. Ishiguro, K. Wang, W. Terashima, H. Fujishiro and H. Hirayama, *J. Cryst. Growth*, 2019, **510**, 47–49.
75 H. Hirayama, W. Terashima, S. Toyoda and N. Kamata, presented in part at the *74th Annual Device Research Conference (DRC)*, 2016.
76 S. Fathololoumi, E. Dupont, C. W. I. Chan, Z. R. Wasilewski, S. R. Laframboise, D. Ban, A. Matyas, C. Jirauschek, Q. Hu and H. C. Liu, *Opt. Express*, 2012, **20**, 3866.
77 A. T. Sarwar, B. J. May, M. F. Chisholm, G. J. Duscher and R. C. Myers, *Nanoscale*, 2016, **8**, 8024–8032.
78 Z. R. Wasilewski, G. C. Aers, A. J. SpringThorpe and C. J. Miner, *J. Vac. Sci. Technol., B: Microelectron. Nanometer Struct.–Process., Meas., Phenom.*, 1991, **9**, 120–131.
79 K. A. Bertness, N. A. Sanford and A. V. Davydov, *IEEE J. Sel. Top. Quantum Electron.*, 2011, **17**, 847.
80 V. Consonni, *Phys. Status Solidi RRL*, 2013, **7**, 699–712.

81 H. Li, L. Geelhaar, H. Riechert and C. Draxl, *Phys. Rev. Lett.*, 2015, **115**, 085503.
82 V. Consonni, M. Knelangen, L. Geelhaar, A. Trampert and H. Riechert, *Phys. Rev. B: Condens. Matter Mater. Phys.*, 2010, **81**, 085310.
83 B. Gunning, J. Lowder, M. Moseley and W. Alan Doolittle, *Appl. Phys. Lett.*, 2012, **101**, 082106.
84 E. Iliopoulos and T. D. Moustakas, *Appl. Phys. Lett.*, 2002, **81**, 295.
85 Q. Zhang, H. Yuan, M. F. Vafadar, G. A. Botton and S. Zhao, *Cryst. Growth Des.*, 2024, **24**, 5263–5268.
86 S. Zhao, S. Y. Woo, M. Bugnet, X. Liu, J. Kang, G. A. Botton and Z. Mi, *Nano Lett.*, 2015, **15**, 7801–7807.
87 M. Belloeil, B. Gayral and B. Daudin, *Nano Lett.*, 2016, **16**, 960–966.
88 K. Hestroffer and B. Daudin, *J. Appl. Phys.*, 2013, **114**, 244305.
89 M. F. Vafadar, Q. Zhang and S. Zhao, *Cryst. Growth Des.*, 2023, **23**, 3091–3097.
90 Y. Taniyasu, M. Kasu and T. Makimoto, *Nature*, 2006, **441**, 325–328.
91 S. Zhao, M. Djavid and Z. Mi, *Nano Lett.*, 2015, **15**, 7006.
92 S. Zhao, S. Y. Woo, S. M. Sadaf, Y. Wu, A. Pofelski, D. A. Laleyan, R. T. Rashid, Y. Wang, G. A. Botton and Z. Mi, *APL Mater.*, 2016, **4**, 086115.
93 Q. Li, Y. Lin, J. R. Creighton, J. J. Figiel and G. T. Wang, *Adv. Mater.*, 2009, **21**, 2416–2420.
94 A. Zhong and K. Hane, *Nanoscale Res. Lett.*, 2012, **7**, 686.
95 X. Yin, Q. Zhang and S. Zhao, *Cryst. Growth Des.*, 2021, **21**, 3645.
96 Q. Zhang, H. Parimoo, E. Martel and S. Zhao, *Sci. Rep.*, 2022, **12**, 7230.
97 Y. Wu, Y. Wang, K. Sun, A. Aiello, P. Bhattacharya and Z. Mi, *J. Cryst. Growth*, 2018, **498**, 109–114.
98 B. J. May, E. C. Hettiaratchy, B. Wang, C. M. Selcu, B. D. Esser, D. W. McComb and R. C. Myers, *Phys. Status Solidi RRL*, 2024, **18**, 2300399.
99 F. Limbach, C. Hauswald, J. Lahnemann, M. Wolz, O. Brandt, A. Trampert, M. Hanke, U. Jahn, R. Calarco, L. Geelhaar and H. Riechert, *Nanotechnology*, 2012, **23**, 465301.
100 A. L. Bavencove, G. Tourbot, J. Garcia, Y. Desieres, P. Gilet, F. Levy, B. Andre, B. Gayral, B. Daudin and L. S. Dang, *Nanotechnology*, 2011, **22**, 345705.
101 W. Y. Fu and H. W. Choi, *Phys. Status Solidi RRL*, 2022, **16**, 2100628.
102 M. F. Vafadar, R. B. Arif, Q. Zhang and S. Zhao, *J. Vac. Sci. Technol., B: Nanotechnol. Microelectron.: Mater., Process., Meas., Phenom.*, 2023, **41**, 030601.

